Enhanced Heat Transfer, 1999, Vol. 6, pp. 161–178
Reprints available directly from the publisher
Photocopying permitted by license only

Horizontal Convective Condensation of Alternative Refrigerants Within a Micro-Fin Tube

M. A. KEDZIERSKI[a,*] and J. M. GONCALVES[b]

[a] *National Institute of Standards and Technology, Gaithersburg, MD 20899;*
[b] *NIST Guest Researcher from Escola Tecnica Federal de Santa Catarina - UnED/SJ, R. Jose Lino Kretzer, 608, Praia Comprida, Sao Jose, S.C., 88.103-902, Brazil*

(Received 14 July 1998; In final form 24 September 1998)

This paper presents local convective-condensation measurements for four refrigerants: R134a, R410A (R32/R125, 50/50% mass), R125, and R32 in a micro-fin tube.[1] Both heat transfer and pressure drop measurements are provided. The heat transfer degradation associated with R410A was shown to be relatively small and believed to be mostly due to nonlinear property effects. The measured convective-condensation Nusselt numbers for all of the test refrigerants were correlated to a single expression consisting of a product of dimensionless properties. The correlation was shown to predict some existing data from the literature within acceptable limits. The correlation poorly predicted the heat transfer performance of cross-grooved, micro-fin tubes. The pressure drop measurements for the micro-fin tube were predicted satisfactorily by an existing correlation for flow-boiling pressure drop in a smooth tube. Correlation of the pressure drop measurements suggested that the heat transfer enhancement was due to the fins behaving as a surface roughness.

Keywords: Enhanced heat transfer, micro-fin, refrigerant mixtures, fluid heating, condensation, pressure drop

INTRODUCTION

Most evaporators and condensers of new unitary refrigeration and air-conditioning equipment are manufactured with micro-fin tubes. The micro-fin tube dominates unitary equipment design because it provides the highest heat transfer with the lowest pressure drop of the commercially available internal enhancements (Webb, 1994). Together, R134a, R22, and R22 replacements constitute by mass nearly all the refrigerants used in unitary products (Muir, 1989). Consequently, two-phase

* Corresponding author.

[1] In order to describe materials and experimental procedures adequately, it is occasionally necessary to identify commercial products by manufacturers' name or label. In no instance does such identification imply endorsement by the National Institute of Standards and Technology, nor does it imply that the particular product or equipment is necessarily the best available for the purpose.

heat transfer data for the micro-fin tube with R134a, R22, and R22 replacements are essential for the design of evaporators and condensers for unitary applications.

Although the study of R134a, R22 and R22 replacements in micro-fin tubes is important, the work available in the open literature is limited. For example, there are surprisingly few studies on R22 replacements and micro-fin tubes. Wang *et al.* (1996) present quasi-local condensation heat transfer coefficients for R22 and R407C. Also, Kaul *et al.* (1996) present local flow-boiling heat transfer measurements for R410B and R407C. Most of the available literature focuses on the heat transfer of R134a and R22. A survey by Schlager *et al.* (1990), which was later updated by Eckels *et al.* (1992), on all the refrigerant heat transfer with micro-fin tubes, showed that of the 22 studies, five were with R113, 15 were with R22, and two examined both fluids. The survey also revealed that condensation research has been neglected relative to evaporation research. For example, 17 of the surveyed studies did not investigate condensation. With help from the Bergles *et al.* (1995) survey and our own search, we were able to find only ten additional papers on convective condensation in micro-fin tubes. Four of these studies were for R134a, five were for R22, and one was the Wang *et al.* (1996) paper on R407C. Most of the recent R134a studies were of global heat transfer measurements as done by Eckels *et al.* (1994). However, only four studies – Chamra and Webb (1995), Chiang (1993), Mori and Nakayama (1983), and Khanpara *et al.* (1986) – present local condensation measurements in a micro-fin tube.

Local condensation measurements will prove most useful to the refrigeration industry. An accurate sizing of a condenser with micro-fin tubes requires an accurate local heat transfer correlation. Unfortunately, neither Ghaderi *et al.* (1995) nor Webb (1994) were able to find a convective-condensation correlation for the micro-fin tube in the literature. The absence of a universal condensation correlation may be partly due to the many variants of the micro-fin geometry and the common practice of using the root diameter area instead of the actual surface area and the hydraulic diameter to calculate the heat transfer. Although the use of the root diameter is convenient, it has little relevance to heat transfer. On the other hand, it may be possible to develop a single local heat transfer expression that can be used for different micro-fin geometries by correlating with respect to the actual surface area and the hydraulic diameter of the tube.

Considering the shortage of convective-condensation data for R22 replacements in a micro-fin tube and the absence of a heat transfer correlation, there were two main objectives of the investigation. The first was to characterize the convective-condensation performance of two R22 alterna- tives in a micro-fin tube. Specifically, the local convective-condensation pressure drop and heat transfer coefficient of R134a and the near-azeotropic refrigerant mixture R410A along with its pure components R32 and R125 were experimentally determined. The experimental measurements for the fluids were correlated to a single correlation as a function of non-dimensional parameters. The second objective was to fundamentally characterize the heat transfer degradation of R410A relative to the performance of the pure components. Convective-condensation heat transfer coefficients for the mixtures' pure components were measured to establish a baseline for the heat transfer degradation calculations. A fundamental understanding of mixture heat transfer mechanisms can be used to refine the selection of mixture composition and/or mixtures for alternative refrigerants.

EXPERIMENTAL APPARATUS

Figure 1 shows a sketch of the experimental apparatus used to establish and measure the convective-condensation heat transfer. The refrigerant flow rate, pressure, and superheat were fixed at the inlet to the test section. The water flow rate and the inlet temperature were fixed to establish the overall refrigerant quality change in the test section.

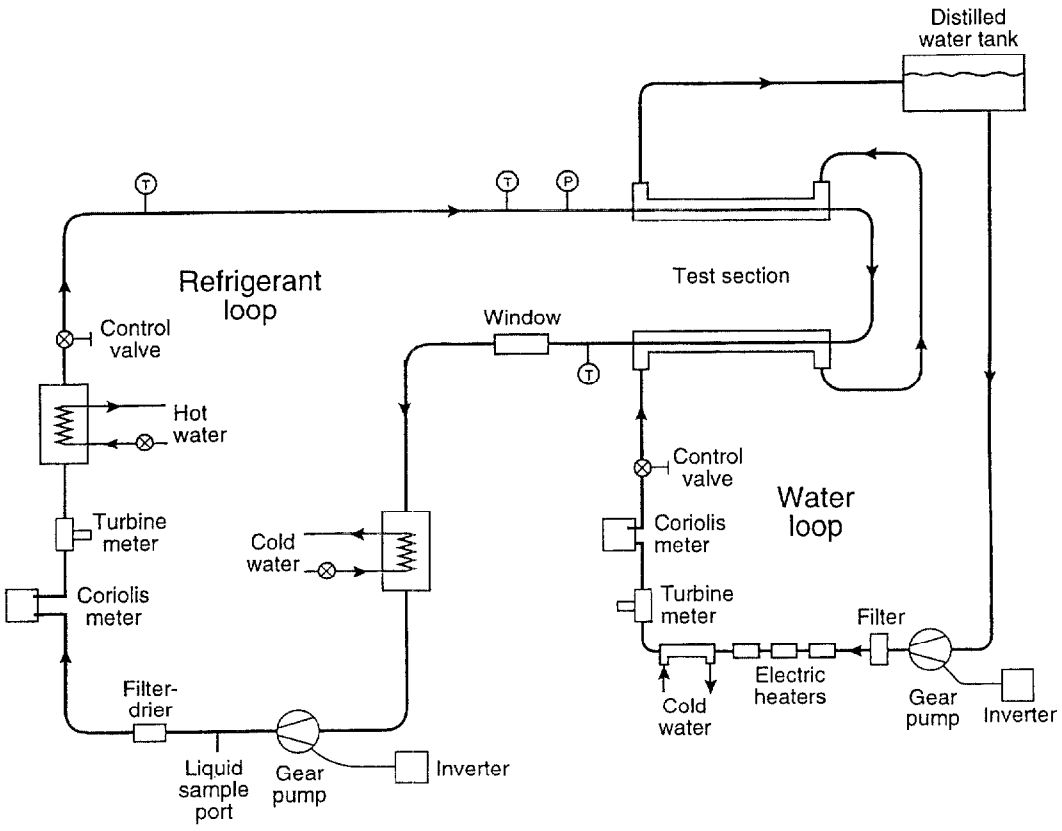

FIGURE 1 Schematic of test rig.

The water temperature drop, the tube wall temperature, the refrigerant temperatures, pressures, and pressure drops were measured at several axial locations along the test section. These measurements were used to calculate the local heat transfer coefficient for the micro-fin tube.

The test section consisted of a pair of 3.34 m long, horizontal tubes connected by a U-bend. A fixed test pressure was maintained by balancing the refrigerant duty between the subcooler, the test section, and the evaporator. A magnetically coupled gear pump delivered the test refrigerant to the entrance of the test section with a few degrees of vapor superheat. Another magnetically coupled gear pump supplied a steady flow of water to the test section. The inlet temperature of the water loop was held constant for each test with a water-chilled heat exchanger and variable electric heaters. The refrigerant and water flow rates were controlled by varying the pump speeds using frequency inverters. Redundant flow-rate measurements were made with Coriolis flowmeters and with turbine flowmeters for both the refrigerant and water sides.

Figure 2 shows a cross section of the test section with a detail of the micro-fin tube geometry. The test refrigerant flowed inside a micro-fin tube, while distilled water flowed either in counterflow or parallel flow to the refrigerant in the annulus that surrounded the micro-fin tube. The annulus gap was 2.2 mm, and the micro-fin tube wall thickness was 0.3 mm. The micro-fin tube had 60, 0.2 mm high fins. The perimeter of one fin and one channel (S) measured perpendicularly to the fin axis was approximately 0.71 mm. The fins rifled down the axis of the tube at a helix angle of 18°

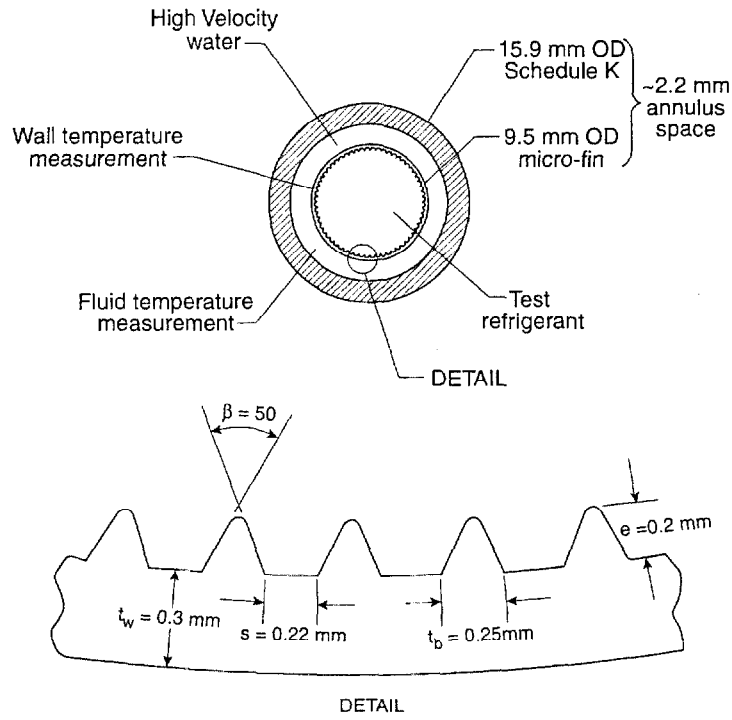

FIGURE 2 Test section cross section.

with respect to the tube axis. For this geometry, the cross-sectional flow area was 60.8 mm^2 giving an equivalent smooth diameter (D_e) of 8.8 mm. The root diameter of the micro-fin tube was 8.91 mm. The inside-surface area per unit length of the tube was estimated to be 44.6 mm. The hydraulic diameter (D_h) of the micro-fin tube was estimated to be 5.45 mm. The ratio of the inner surface area of the micro-fin tube to the surface area of a smooth tube of the same D_e was 1.6.

Figure 3 provides a detailed schematic of the test section. The annulus was constructed by connecting a series of tubes with 14 pairs of stainless steel flanges. This construction permitted the measurement of both the outer micro-fin wall temperature and the water temperature drop as discussed in the following two paragraphs. The design also avoided abrupt discontinuities such as unheated portions of the test section and tube-wall "fins" between thermopile ends.

Figure 3 also shows that thermocouple wires pass between 12 of the gasketed flange pairs to measure the refrigerant-tube wall temperature at ten locations on the top, side, and bottom of the tube wall. These locations were separated by 0.6 m on average, and they were located near the intersection of the shell flanges. In addition to these, thermocouples were also mounted near the middle pressure taps. The thermocouple junction was soldered to the outside surface and was sanded to a thickness of 0.5 mm. The leads were strapped to a thin non-electrically-conducting epoxy layer on the wall for a distance of 14.3 mm before they passed between a pair of the shell flanges. The wall temperature was corrected for a heat flux dependent fin effect. The correction was typically 0.05 K.

A chain of thermopiles is shown in Figure 3 that was used to measure the water temperature drop between each flange location. Each thermopile consisted of ten thermocouples in series, with the

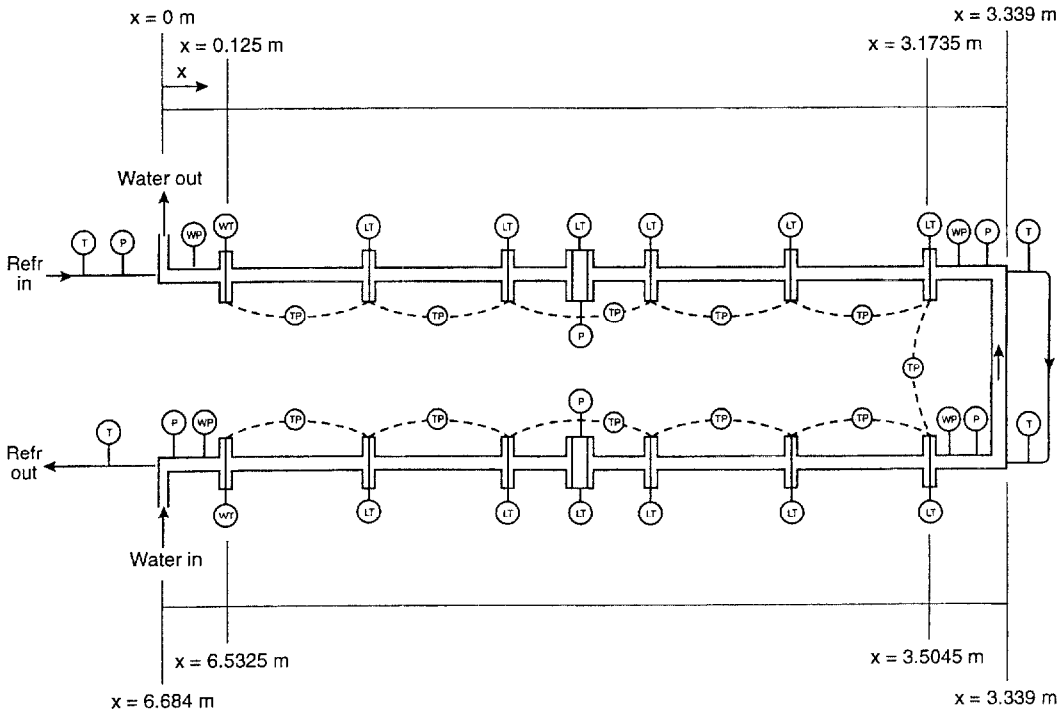

FIGURE 3 Detailed schematic of test section.

ten junctions at each end evenly spaced around the circumference of the annulus. Because the upstream junctions of one thermopile and the downstream junctions of another enter the annulus at the same axial location (except at the water inlet and outlet), the junctions of the adjacent piles were alternated around the circumference. A series of teflon half-rings attached to the inner refrigerant tube centered the tube in the annulus. The half-rings were circumferentially baffled to mix the water flow. Mixing was further ensured by a high water Reynolds number (Kattan *et al.*, 1995).

As shown in Figure 3, six refrigerant pressure taps along the test section allowed the measurement of the upstream absolute pressure and five pressure drops along the test section. Two sets of two water pressure taps were used to measure the water pressure drop along each tube. Also, a sheathed thermocouple measured the refrigerant temperature at each end of the two refrigerant tubes, with the junction of each centered radially. Only the thermocouple at the inlet of the first tube was used in the calculations. The entire test section was wrapped with 5 cm of foam insulation to minimize heat transfer between the water and the ambient.

HEAT TRANSFER COEFFICIENTS

The convective-condensation heat transfer coefficient based on the actual inner surface area ($h_{2\phi}$) was calculated as:

$$h_{2\phi} = \frac{q''}{T_r - T_w} \tag{1}$$

where the measured wall temperatures (T_w) were fitted to their axial position to reduce the uncertainty in the measurement. The best fits for the wall temperature for parallel flow and counterflow differed. The measured wall temperatures for

counterflow were fitted to:

$$T_w = A_0 + A_1 z^2 \tag{2}$$

The measured wall temperatures for parallel flow were fitted to:

$$T_w = A_0 + A_1 z + A_2 z^2 \tag{3}$$

The uncertainty of most of the fitted wall temperatures was less than 0.5 K. The median of the uncertainty in T_w as shown in Table I was 0.35 K. Further detail on the wall-temperature uncertainty is given in Kedzierski and Goncalves (1997).

The water temperature (T_f) was determined from the measured temperature change obtained from each thermopile and the inlet water-temperature measurement. The water temperature was regressed to the axial location of the thermopiles along the z-coordinate. As shown for the T_w regressions, the best fits for the water temperatures differed for parallel flow and counterflow. The water temperatures for counterflow were fitted to:

$$T_f = A_0 + A_1 z^2 + A_2 z^3 \tag{4}$$

The measured water temperatures for parallel flow were fitted to:

$$T_f = A_0 + A_1 z + A_2 z^2 + A_3 z^3 \tag{5}$$

TABLE I Median estimated 95% relative expanded uncertainties for Eq. (10) data

Parameter	Minimum	Maximum	U%
G_r [kg/m^2·s]	57	552	2.0
T_r [K]	293.0	323.0	0.1 (0.3 K)
P [kPa]	600	2000	1.5
T_w [K]	288.0	318.0	0.1 (0.357 K)
$\dot{m}_f$ [kg/s]	0.0150	0.0450	2.0
T_f [K]	278.0	313.0	0.1
P_f [kPa]	200	110	1.0
q'' [kW/m^2]	0.72	39	5.1
dT_f/dz [K/m]	0.014	0.57	5.2
ΔT_s [K]	0.41	12.6	15.2 (0.44 K)
Nu	58	508	16.4
Re	3500	24000	4.0
Ja	6	256	16.0
Pr	1.7	3.6	2.0
P_r/Pc	0.22	0.62	2.0
Sv	0.86	10.3	3.0
x_q	0.06	1.0	8.0

The water-temperature fits, the measured water mass flow rate ($\dot{m}_f$), and the properties of the water were used to calculate the local heat flux (q'') to the micro-fin tube based on the actual inner surface area:

$$q'' = \frac{\dot{m}_f}{p}\left(c_{p_f}\frac{dT_f}{dz} + \nu_f \frac{dP_f}{dz}\right) \tag{6}$$

where p is the wetted perimeter of the inside of the micro-fin tube. The specific heat (c_p) and the specific volume (ν_f) of the water were calculated locally as a function of the water temperature. The local, axial water-temperature gradient (dT_f/dz) was calculated from a derivative of either Eq. (4) or (5) depending on the corresponding flow configuration. The water pressure gradient (dP_f/dz) was linearly interpolated between the pressure taps to the location of the wall thermocouples. The pressure gradient term was typically less than 3% of the temperature gradient term.

Figure 4 shows an example plot of the local heat flux as calculated from Eq. (6) *versus* the thermodynamic quality. Counterflow and parallel flow heat flux profiles are compared for R134a at a Reynolds number of 15100 and a refrigerant pressure of 1160 kPa. The form of the counterflow and parallel flow differ, as suggested by the use of two different water-temperature fits for the two

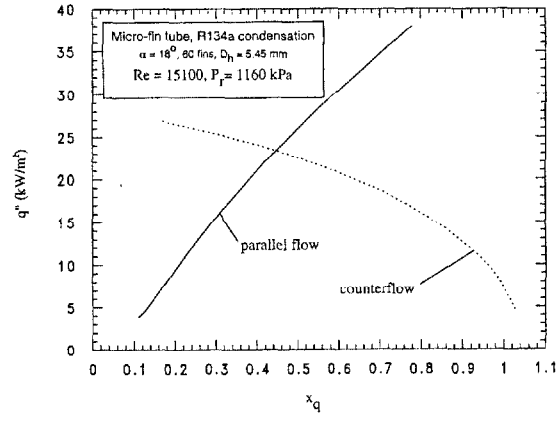

FIGURE 4 Comparison of counterflow and parallel flow heat flux distributions.

flow conditions. The two flow conditions provided for a wider range of heat fluxes at a given thermodynamic quality. In this way, the sensitivity of the heat transfer coefficient to the heat flux could be thoroughly investigated as a function of quality.

The equilibrium refrigerant temperature (T_r) and all other thermodynamic and transport properties were calculated with version five of REFPROP (Huber *et al.*, 1995) with enthalpy and pressure as inputs. The enthalpy of the refrigerant vapor at the inlet of the test section was calculated from its measured temperature and pressure. The subsequent drop in refrigerant enthalpy along the test section was calculated from the local heat flux and the measured refrigerant mass flow rate. The refrigerant pressures were measured at six pressure taps along the test section. The pressure was linearly interpolated between the taps. The average T_r was varied between 30°C and 50°C with approximately 5 K of superheat at the test section inlet.

The local Nusselt number (Nu) was calculated based on the actual inner surface area of the tube as:

$$\mathrm{Nu} = \frac{h_{2\phi} D_h}{k_l} \tag{7}$$

Testing the two flow conditions also benefitted the correlation of data by providing complimentary uncertainty profiles with thermodynamic quality. For example, the uncertainty of the low quality, parallel flow Nusselt number data exhibits high uncertainties, while the low quality, counterflow data exhibits low uncertainties. Consequently, by testing with both flow conditions, much of the parallel flow data can be omitted from the correlation due to its high uncertainty, while still maintaining sufficient counterflow data in the low quality region to produce a valid correlation. A similar, but opposite, scenario exists in the high-quality region.

The cubic fit of the wall- and water-temperature profiles were within ±0.8 K and ±0.2 K, respectively, of the measured temperatures. On average, the residual standard deviation of the wall- and water-temperature fits was 0.5 K and 0.1 K, respectively. The refrigerant temperatures were obtained from pressure measurements and the REFPROP (Huber *et al.*, 1995) equation of state.

Figure 5 provides corroboration of the present local heat-flux and wall-temperature measurements with the Wiegand (1945) correlation for single phase turbulent heat transfer in a smooth annulus. The local heat flux, measured wall and water temperatures were used to calculate the local water-side heat transfer coefficient for the annulus. Figure 5 shows that approximately 80% of the measured water-side heat transfer coefficients are within ±25% of the Wiegand (1945) correlation. The range of the difference between measurements and Wiegand's (1945) correlation is nearly centered about the correlation and lies within ±36% which was the range given by E. L. McMillen for his data in the "Written Discussion" section of Wiegand's (1945) paper. This provides an independent validation of the wall temperature and heat flux measurements.

Table I shows the expanded measurement uncertainty (U) of the various measurements along with the range of each parameter in this study. The U was estimated with the law of propagation of uncertainty. All expanded measurement uncertainties are reported for a 95% confidence interval and are evaluated by statistical methods. The estimates

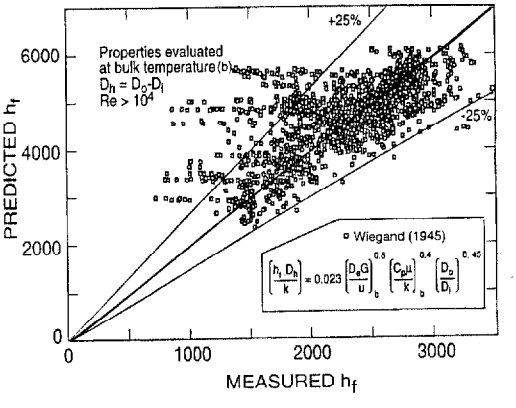

FIGURE 5 Corroboration of measurement procedure.

shown in Table I are median values of U for the correlated data. More detail on the various uncertainties is given in Kedzierski and Goncalves (1997).

RESULTS

The 1704 heat transfer and pressure drop data points generated in this study for R32, R125, R410A, and R134a are tabulated in the appendices of Kedzierski and Goncalves (1997).

Heat Transfer

The present heat transfer measurements concur with the approximate magnitude of the heat transfer enhancement reported by Webb (1994). Webb (1994) states that the micro-fin tube provides anywhere from 100% to 200% improvement over smooth-tube R22 condensation performance. Figure 6 shows a graph of the condensation heat transfer enhancement ratio (E_h),

$$E_h = \frac{h_{2\phi} A_i}{h_p \pi D_e L} \tag{8}$$

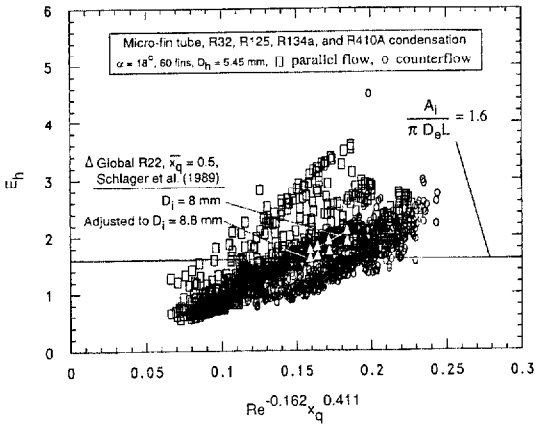

FIGURE 6 Condensation heat transfer enhancement ratio for micro-fin tube.

versus Reynolds number. The heat transfer coefficient of the plain surface (h_p) was calculated from the smooth-tube convective-condensation correlation of Ackers and Rosson (1960) using the equivalent diameter (D_e) to calculate the Reynolds and Nusselt numbers. The h_p was calculated using the same mass velocity and fluid properties that were used for the experimental data.

The enhancement ratio shown in Figure 6 varies from approximately 0.6 to 3.6 for the micro-fin tube. Approximately half of the enhancement factors are greater than 1.6. Enhancement ratios below 1.6 indicate that the micro-fin heat transfer coefficient based on the surface area is less than that of a smooth tube. Enhancement ratios greater than 1.6 suggest that the enhancement caused by the micro-fin surface is due to more than just the 60% surface area increase over the smooth surface with the same cross sectional flow area.

Regression of dimensionless parameters against E_h was used to assist in the investigation of the mechanism that was responsible for the heat transfer enhancement. The E_h was found to be primarily a function of Reynolds number and thermodynamic quality:

$$E_h = 9.777\ \mathrm{Re}^{-0.162}\ x_q^{0.411} \tag{9}$$

The relative magnitude of the exponents in Eq. (9) shows that the quality has more influence on the E_h than does the Re. The negative exponent on the Reynolds number shows that the effectiveness of the micro-fin enhancement mechanism decreases for increasing Reynolds numbers. Conversely, Eq. (9) shows that the micro-fin enhancement mechanism is more effective for larger values of quality. The enhancement mechanism with respect to increasing quality may result from an interaction between the fins and the liquid–vapor interface of the fluid in the tube. At very high vapor qualities and very thin liquid films on the surface, the fins may be very effective at mixing the liquid–vapor interface due to their proximity to the liquid–vapor interface. It is also possible to obtain an additional enhancement at

very high qualities from surface-tension drainage forces on the fin-tips. However, as the liquid accumulates on the surface, both the liquid – vapor interface mixing and the surface-tension effects diminish. Consequently, the E_h is larger at higher qualities. The heat transfer enhancement with respect to the Reynolds number may result from an interaction between the fins and the turbulence in the liquid film. Smaller eddies transfer momentum more efficiently than larger eddies. Low Reynolds number flows may be enhanced more readily than high Reynolds number flows due to the reduction in the size of the turbulent eddies at the wall by the interaction of the flow with the fins. High Reynolds number flows are not enhanced as readily as low Reynolds number flows because there are fewer large eddies to be reduced at higher Reynolds numbers.

The enhancement ratio that Schlager *et al.* (1989) obtained for the same micro-fin tube as used in this study is presented as solid, white lines in Figure 6. They used a global micro-fin heat transfer coefficient measurement over a 0.6 to 0.8 quality change to calculate E_h. For the reference case, Schlager *et al.* (1989) measured smooth-tube heat transfer coefficients for an 8 mm inner diameter tube. The solid white line shows the enhancement ratio as reported by Schlager *et al.* (1989) using the 8 mm diameter tube in its calculation. The dashed line shows the E_h after the smooth-tube conductance was multiplied by $(8/8.8)^{0.8}$ to convert to an E_h based on a 8.8 mm smooth inner diameter, *i.e.*, D_e for the micro-fin tube. The Reynolds number and quality dependence of the Schlager *et al.* (1989) E_h roughly agrees with the present E_h measurement. The slope of the Schlager *et al.* (1989) is consistent with the mean slope of the measurements. Considering that the Schlager *et al.* (1989) E_h is for average heat transfer conditions, their data would be expected to lie close to the middle of the data range. The Schlager *et al.* (1989) enhancement ratio that was adjusted to the 8.8 mm diameter lies relatively close to the median of the data.

Figure 7 includes a comparison of the experimental micro-fin Nusselt numbers to the smooth-tube convective-condensation correlation of Ackers and Rosson (1960) using the hydraulic diameter to calculate the Reynolds and Nusselt numbers. The figure shows that use of the hydraulic diameter in a smooth-tube condensation correlation predicts most of the micro-fin data to within +20% and −40%. The majority of the data is under-predict with the Ackers and Rosson (1960) correlation. Apparently, the smooth-tube correlation does not account for the flow enhancement provided by the fins. Consequently, a new correlation is needed to account for the heat transfer enhancement due to the micro fins.

The convective-condensation Nusselt numbers (Nu) were correlated following the law of Corresponding States philosophy presented by Cooper (1984). Cooper (1984) suggested that the fluid properties that govern nucleate pool boiling can be well represented by a product of the reduced pressure (P_r/P_c), the acentric factor $(-\log_{10}(P_r/P_c))$, and other dimensionless variables to various powers. The above reduced-pressure terms and several other locally evaluated terms were used to correlate the measured local Nu for all condensing flow conditions and refrigerants

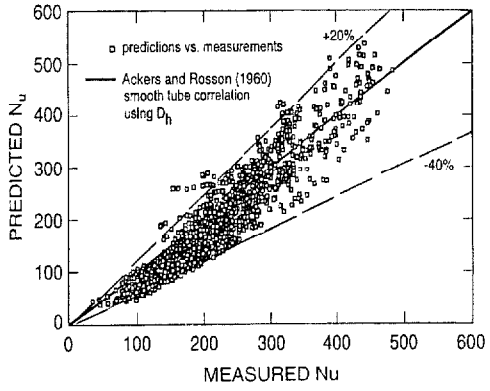

FIGURE 7 Comparison of measured convective condensation Nusselt numbers to those predicted with Ackers and Rosen (1960) using D_h.

in this study to:

$$\mathrm{Nu} = \frac{h_{2\phi} D_h}{k_l} = 2.256\ \mathrm{Re}^{\beta_1}\ \mathrm{Ja}^{\beta_2}\ \mathrm{Pr}^{\beta_3} \left(\frac{P_r}{P_c}\right)^{\beta_4} \left(-\log_{10}\frac{P_r}{P_c}\right)^{\beta_5} Sv^{\beta_6}$$

where:

$$\beta_1 = 0.303$$
$$\beta_2 = 0.232 x_q$$
$$\beta_3 = 0.393$$
$$\beta_4 = -0.578 x_q^2$$
$$\beta_5 = -0.474 x_q^2$$
$$\beta_6 = 2.531 x_q \qquad (10)$$

where the Reynolds number (Re), the Jakob number (Ja), the Prandtl number (Pr), the reduced pressure (P_r/P_c), the dimensionless specific volume (Sv) and the quality (x_q) are all evaluated locally at the saturated condition.

Baker's (1954) flow map and Soliman's (1982, 1983, and 1986) flow transition correlations for smooth tubes were used to approximately determine the flow conditions. Baker's results showed that 79%, 18%, 2%, and 1% of the data were in annular, slug, bubbly, and wavy flow, respectively. Soliman's correlations indicated that 47%, 30%, and 23% of the data were in wavy (stratified, slug and wavy), annular, and mist flow, respectively. No reduction in the residual standard deviation of the Nu regression was obtained when the data set was reduced to only the annular flow (as indicated by the Soliman correlations) data.

The search for the above form of the correlation began with quadratic exponents in quality for each dimensionless variable. The quadratic exponent form was used with good results by Kedzierski and Kim (1998) to correlate several other pure refrigerants and mixtures for a wide range of qualities for both evaporative and condensing flows. The number of dimensionless variables and constants in the exponents were reduced to only those with significant influence on the residual standard deviation of the fit. For example, because R410A is a near-azeotrope, the composition difference between vapor and liquid phases had a negligible influence on the fit of the correlation. Consequently, the composition difference was not used in the fit of the data.

One-thousand-and-sixty-seven data points out of the total 1704 data points were used in the regression of Eq. (10). Measurements with large uncertainties, and measurements that had high influence, or high leverage on the model were all candidates for exclusion from the regression. Data were excluded from the regression only when it could be justified. The details of the data filtering procedure are given in Kedzierski and Goncalves (1997).

Figure 8 compares the measured condensation Nusselt numbers for the micro-fin tube to the Nusselt numbers predicted with Eq. (10). Equation (10) correlates 95% of the pure-component and near-azeotropic convective-condensation Nusselt numbers to within approximately ±21%. The mean of the correlation has an average uncertainty of ± 3% over the entire range of Nusselt numbers. Only random trends were observed in the residual plots against each of the parameters of Eq. (10). The residual standard deviation of Eq. (10) and that for the separate fits for each fluid were nearly the same. This suggests that the scatter in the data is not caused by the different fluids.

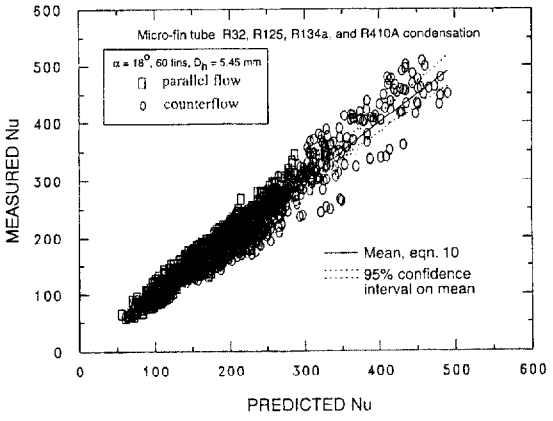

FIGURE 8 Comparison of measured and predicted convective condensation Nusselt numbers.

A simpler form of Eq. (10) with a larger uncertainty is:

$$\mathrm{Nu} = \frac{h_{2\phi} D_h}{k_l} = 4.94\ \mathrm{Re}^{\beta_1}\ \mathrm{Pr}^{\beta_3} \left(\frac{P_r}{P_c}\right)^{\beta_4} \left(-\log_{10}\frac{P_r}{P_c}\right)^{\beta_5} Sv^{\beta_6}$$

where

$$\beta_1 = 0.235$$
$$\beta_3 = 0.308$$
$$\beta_4 = -1.16x_q^2$$
$$\beta_5 = -0.887x_q^2$$
$$\beta_6 = 2.708x_q \qquad (11)$$

Equation (11) does not require an iteration procedure on the ΔT_s to evaluate the Jakob number. However, the uncertainty of fit is approximately 23.5% which is larger than that of Eq. (10).

Figure 9 shows the heat transfer coefficient *versus* quality for each of the four test fluids at $T_r = 40°\mathrm{C}$, $\Delta T_s = 5\,\mathrm{K}$, and $G_r = 250\,\mathrm{kg/(m^2 \cdot s)}$. The solid lines are predictions for the present micro-fin tube geometry which were obtained from the correlation of the data given as Eq. (10). In general, the measured condensation heat transfer coefficient decreases for decreasing qualities. Apparently, thin liquid films and high vapor velocities at the entrance of the tube provide for high heat transfer coefficients. As the liquid accumulates on the tube wall for decreasing quality, the heat transfer coefficient diminishes. The refrigerant R32 exhibits the highest heat transfer performance of the four test fluids. R32 owes much of its heat transfer performance to its high thermal conductivity. As expected, the performance of the near-azeotropic mixture, R410A, is between that of its pure components, R32 and R125. The predicted performance of R22 is near that of its proposed replacement, R410A. The R125 exhibits lower condensation Nusselt numbers than that for R134a for the above conditions. Conversely, as shown by Kaul *et al.* (1996), the flow-boiling performance of R125 is greater than that of R134a in the identical tube.

Over 140 figures would be required to depict the Nusselt number *versus* thermodynamic-quality relationships for each test. Consequently, only representative plots of Nu *versus* x_q are given in Figures 10 through 13. Each figure compares counterflow to parallel flow for nominally the same Reynolds number and reduced pressure. The solid lines are predictions for the present micro-fin tube geometry which were obtained from the correlation of the data given as Eq. (10). The

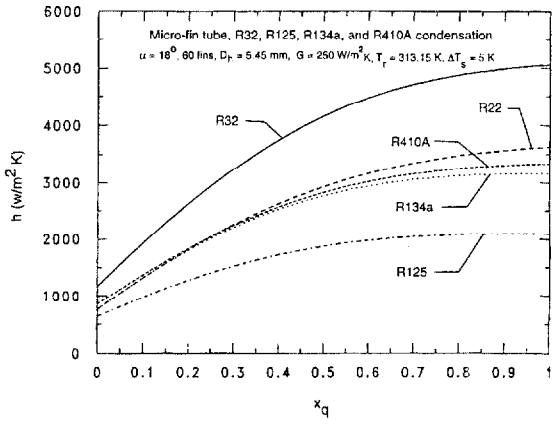

FIGURE 9 Comparison of the heat-transfer coefficient for different fluids *versus* thermodynamic quality.

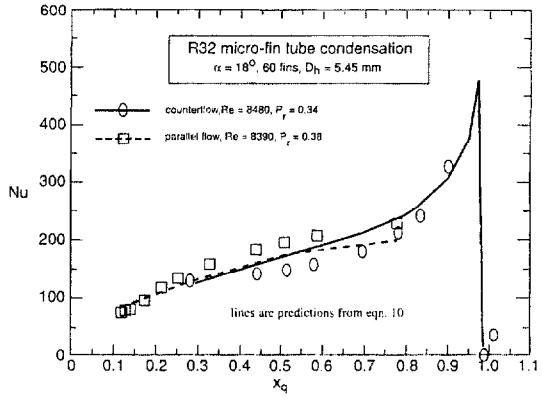

FIGURE 10 Condensation Nusselt number *versus* thermodynamic quality for R32.

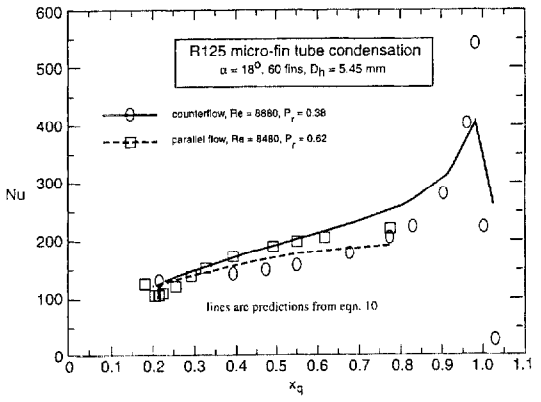

FIGURE 11 Condensation Nusselt number *versus* thermodynamic quality for R125.

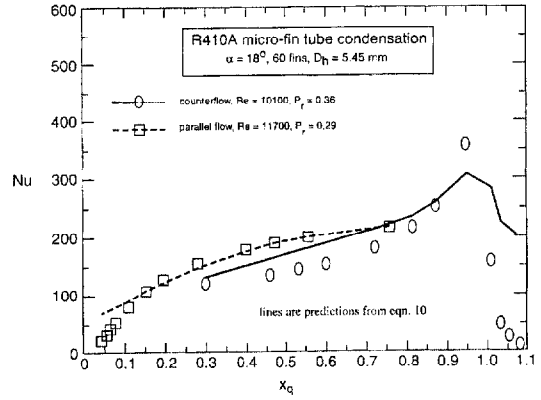

FIGURE 12 Condensation Nusselt numbers *versus* thermodynamic quality for R140A.

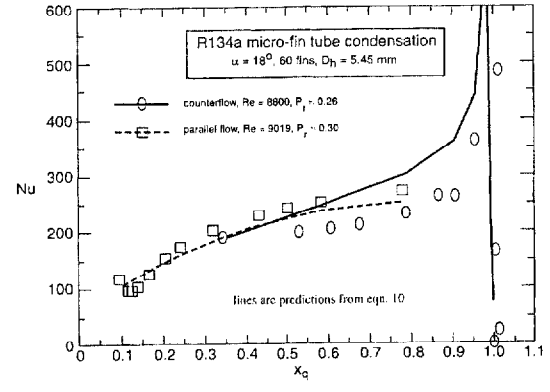

FIGURE 13 Condensation Nusselt number *versus* thermodynamic quality for R134a.

symbols are the measured data points. In general, parallel flow exhibits larger Nusselt numbers for the 0.3 to 0.7 quality range. Below and above this range, the Nusselt numbers for counterflow and parallel flow nearly coincide. Both the Nusselt number measurements and the predictions for counterflow are concave with respect to quality. By contrast, the parallel flow Nusselt number measurements and predictions are convex with respect to quality. The difference in the Nusselt numbers in the mid-quality range may be due to the difference in the heat flux *versus* quality relationship between counterflow and parallel flow. The exact mechanism that is responsible for the difference between counterflow and parallel flow is not fully understood. Although the correlation predicts both the concave and convex trends with respect to quality, it, apparently, does not account for the entire difference between Nusselt numbers for the two flow conditions. Eq. (10) consistently under-predicts the counterflow Nusselt numbers and over-predicts the parallel flow Nusselt numbers.

Figure 14 compares the predictions of Eq. (10) to the local condensation heat transfer data that was available in the literature. All of the heat transfer coefficients taken from the literature were read from graphs and based on the root-diameter area. Consequently, all of the heat transfer

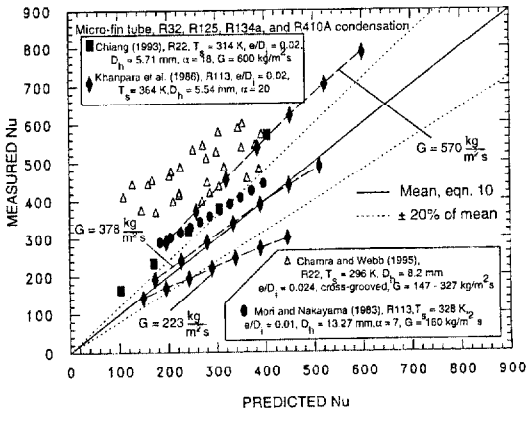

FIGURE 14 Comparison of Eq. (10) to data available in the literature.

coefficients from the literature had to be adjusted so that they were based on the actual inner surface area of the tube in order to compare the literature data with Eq. (10). Cross-sectional schematics and tabulated dimensions of the tubes were used to calculate the surface areas and the hydraulic diameters of the micro-fin tubes from:

$$D_h = \frac{4A_c \cos\alpha}{N_f S} \tag{12}$$

where S is the perimeter of one fin and channel taken perpendicular to the axis of the fin, N_f is the number of fins, A_c is the cross-sectional flow area, and α is the helix angle of the fin.

Mori and Nakayama (1983) measured R113 quasi-local condensation heat transfer coefficients for three different micro-fin tube geometries. The Mori and Nakayama (1983) data for a 20 mm inner diameter tube with 0.2 mm high micro fins at a 7° helix angle are presented as closed circles in Figure 14. The Mori and Nakayama (1983) data presented in Figure 14 are for a mass velocity of 160 kg/m^2· s. Most of this data lies within ± 20% of the predictions. Chiang (1993) graphically presented measured quasi-local condensation heat transfer coefficient for one of four micro-fin tube geometries that he tested. The local heat flux was estimated from $dx_q/dz = 0.09$/m which was given by Chiang (1993). The Chiang (1993) data for R22 in a 10 mm outer diameter tube with 60, 0.18 mm high micro fins at a 18° helix angle and a mass velocity of 600 kg/m^2· s are presented as closed rectangles in Figure 14. Most of the Chiang (1993) data lies just below the 20% under-prediction line. The quasi-local condensation heat transfer measurements of Khanpara *et al.* (1986) for three different mass velocities (223 kg/m^2· s, 378 kg/m^2· s, and 570 kg/m^2· s) are shown as closed diamonds in Figure 14. The local heat flux was estimated from quality change over the test section which was given as from 0.2 to 0.3. The measured Nusselt numbers of Khanpara *et al.* (1986) for their intermediate mass velocity of 378 kg/m^2· s lie very close to those predicted by Eq. (10). However, the high-quality region of the low mass velocity data (223 kg/m^2· s) are over-predicted by more than 20%. Similarly, nearly all of the high mass velocity (570 kg/m^2· s) Nusselt numbers are under-predicted by approximately 30%.

The data from the literature are all within the mass velocity limits for which the correlation was developed. Also, the e/D_i ratios for the tubes from the literature, with the exception of the Mori and Nakayama (1983) data, are approximately equivalent to the present tube (0.02). However, considering the wide range of tube diameters, helix angles, fluids, fin shapes, and estimates made for the literature data, the agreement between Eq. (10) and Nusselt numbers from the literature is to be expected. Also, it is very difficult to estimate the hydraulic diameter not knowing the exact pattern of the fins. This is especially true for the Chiang (1993) data which was for mechanically expanded micro-fin tubes. Certainly, the mechanical expansion process altered the fin profiles and increased the overall diameter of the tube. If a larger hydraulic diameter were to be used in the predictions, the Chiang (1993) agreement between the predictions and measurements would improve.

Although, Eq. (10) predicts the micro-fin data fairly well, the predictions of the cross-grooved micro-fin data of Chamra and Webb (1995) are under-predicted on average by 40%. Possibly, the cross grooves provide an additional enhancement that is not accounted for by Eq. (10). The process of forming the cross groove creates a bump or a spill over into the major groove. The additional enhancement could be due to the high heat transfer that would occur on the leading edge of the bump. Equation (10) cannot account for the enhancement due to the bump. Also, the cross groove tubes were created from flat stock with a "*W*-shaped" fin axis then seam welded. Consequently, the main fin axis of the cross grooved tube did not rifle down the axis. Possibly, the non-spiraling fin also contributed to a difference in performance from the Eq. (10) prediction.

Figure 15 shows the heat transfer degradation ($\Delta h_{2\phi}$) as a function of heat flux for the R410A

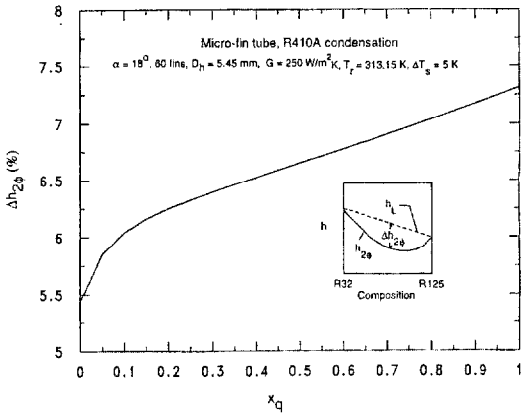

FIGURE 15 Heat transfer degradation for the R410A mixture.

mixture at a mass flux of 246 kg/m^2 s. The $\Delta h_{2\phi}$ was calculated from the correlations using the same definition as given in Kedzierski *et al.* (1992):

$$\Delta h_{2\phi} = h_L - h_{2\phi} \tag{13}$$

where h_L is the heat transfer coefficient obtained from a linear interpolation of the pure components at a given composition. The heat transfer degradation is independent of heat flux and no greater than 2.5%. The average difference between the vapor and liquid concentration was 0.02 mole, suggesting that the degradation was mostly due to property effects.

Pressure Drop

Pierre (1964) developed the following semi-empirical equation to predict the pressure drop for flow boiling in a horizontal smooth tube:

$$\Delta P = \left(0.0185\left(\frac{\Phi}{\mathrm{Re}}\right)^{1/4} + \frac{\Delta x_q D_h}{x_{q_m}\Delta L}\right) \frac{\Delta L}{D_h} G^2 x_{qm} \nu_v \tag{14}$$

where the specific volume of the vapor (ν_v), the Reynolds number, the mass velocity (G), and the two-phase number $\left(\Phi = \frac{\Delta x_q\, i_{fg}}{\Delta L\, g}\right)$ are evaluated at the average temperature of the refrigerant. The average quality over length ΔL is x_{qm}. The above correlation originates from the first law of thermodynamics. The first term within the bracket represents the dimensionless friction factor.

The second term is from the acceleration portion of the pressure drop. Pierre (1964) fitted his pressure drop measurements to Eq. (14) to obtain an expression for the friction factor. With the exception of the friction factor which may be germane to flow boiling, Eq. (14) applies to condensation as well as to evaporation. One might expect that pressure drops due to flow boiling (in the absence of nucleate boiling) and condensation may be governed by the same physical phenomenon. If so, then the Pierre (1964) correlation should work as well for convective condensation as it does for convective evaporation.

Figure 16 compares the micro-fin condensation pressure drop to Pierre (1964) flow-boiling pressure drop correlation. The hydraulic diameter was used in the Pierre (1964) correlation to predict most of the condensation pressure drop measurements in the present micro-fin tube to within ± 20%. Pierre recommends that Eq. (14) not be used for values of (Re/Φ) greater than 1. Only three data points in the data set violated this criteria. Overall, the Pierre (1964) correlation predicts the convective-condensation pressure

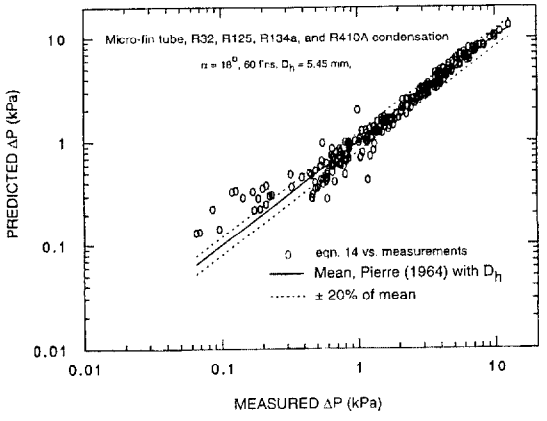

FIGURE 16 Comparison of micro-fin condensation pressure drop to Pierre (1964) boiling pressure drop correlation.

drop measurements for the micro-fin tube acceptably well. However, the mean of the predictions lies slightly below the ideal prediction line.

Following the development of the Pierre (1964) pressure drop equation, the Fanning friction factor for the present data was calculated as:

$$f_r = \frac{D_h}{(\nu_o + \nu_i)\Delta L}\left(\frac{(P_i - P_o)}{G^2} - (\nu_o - \nu_i)\right) \quad (15)$$

where specific volume of the fluid (ν) was calculated from a thermodynamic quality weighted average of the liquid and vapor specific volumes. Only the two central portions of the test section (Fig. 3) were used to ensure that all of the correlated data were for two-phase flow.

In order to center the friction factor predictions about the data, the measured friction factors were regressed to the following:

$$f_r = 0.00228\ \mathrm{Re}^{-0.062}\,\Phi^{0.211} \quad (16)$$

Twenty-six data points were removed from the fit because they had high influence and high leverage on the fit. The deleted data were for somewhat low pressure drop values which are associated with larger relative measurement uncertainties.

The exponent on the two-phase number given in Eq. (16), 0.211, is consistent with that given by Pierre (1964): 0.24. However, the exponent on the Reynolds number, -0.062, is very different from that given by Pierre (1964): -0.24. The exponent on the Reynolds number of Eq. (16) is approximately equivalent to -0.06 which is the exponent that one would calculate from the transition zone of the Moody (1944) chart using the fin height (0.2 mm) for the roughness height. Consequently, the new friction factor should be more appropriate for micro fins because it accounts for the influence of the fins on the flow.

The fact that the Reynolds number exponent is consistent with that obtained from the Moody (1944) chart suggests that the fins of a micro-fin tube act like a roughness to enhance the convective-condensation heat transfer. If roughness mixing dominates the enhancement mechanism, neither swirl effects nor surface-tension drainage have much influence on the heat transfer. The lack of importance of surface-tension and swirl flow may be a consequence of the flow conditions and surface geometry. It may be possible that the roughness effect would not dominate for other flow conditions and micro-fin tubes with larger heights.

The corroboration between the present Re exponent and Moody's (1944) also suggests that the frictional pressure drop of micro-fin tubes should depend on the fin-height-to-root-tube-diameter (e/D_i) ratio. If it is assumed that the fins act purely as a roughness, the Moody (1944) chart can be used to interpolate between the Eq. (16) friction factor and Pierre's (1964) smooth-tube friction factor for a given e/D_i ratio as follows:

$$f_r = \left(0.002275 + 0.00933\exp\left(\frac{e/D_i}{-0.003}\right)\right) \mathrm{Re}^{-1/(4.16+532(e/D_i))}\Phi^{0.211} \quad (17)$$

In the above equation, the functional forms of the leading coefficient and the Reynolds number exponent with respect to e/D_i were determined from the Moody (1944) chart. Also, Pierre's (1964) friction factor equation was modified for use in the interpolation. Namely, the exponent on the two-phase number of Pierre's (1964) friction factor correlation was set equal to that of Eq. (16) and the leading coefficient on Pierre's correlation was adjusted to give approximately the same results, for our data set, as the original equation.

The pressure drop equation for which Eqs. (16) and (17) are valid is:

$$\Delta P = \left(\frac{f_r(\nu_o + \nu_i)\Delta L}{D_h} + (\nu_o - \nu_i)\right)G^2 \quad (18)$$

This is essentially the same equation as given by Pierre (1964) with the exception that the specific volume of the liquid is not neglected. The uncertainty of the fit was reduced when the liquid specific volume was included.

CONCLUSIONS

Local convective-condensation measurements for four refrigerant fluids: R134a, R410A(R32/R125, 50/50%mass), R125, and R32 in a micro-fin tube were presented. Both heat transfer and pressure drop measurements were provided. The measured convective-condensation Nusselt numbers for all of the test refrigerants were correlated to a single expression consisting of a product of dimensionless properties. The correlation was shown to predict existing condensation Nusselt numbers for micro-fin tubes from the literature acceptably well. However, the correlation poorly predicted the Nusselt numbers for micro-fin tubes with cross-grooves. It was speculated that bumps from the cross-grooves caused an additional enhancement that could not be accounted for by the correlation. The hydraulic diameter was used in an existing flow-boiling correlation from the literature to predict most of the condensation pressure drop measurements in the micro-fin tube to within $\pm 20\%$.

In general, the measured condensation heat transfer coefficient decreased with decreasing qualities. The refrigerant R32 exhibited the highest heat transfer performance due to its high thermal conductivity. As expected, the performance of the near-azeotropic mixture R410A was between that of its pure components R32 and R125. The heat transfer degradation associated with R410A was shown to be relatively small and believed to be mostly due to nonlinear property effects.

The enhancement ratio was shown to span from 3.6 at low Re to 0.6 at high Re. It was speculated that the micro fins enhanced the heat transfer with a combination of liquid–vapor interface mixing and turbulent mixing near the wall. The surface behaves as a roughness in the enhancement of the heat transfer. Surface-tension drainage and swirl effects are presumed to have little influence on the heat transfer. At high vapor qualities and thin liquid films on the surface, the fins act to mix the liquid–vapor interface. At lower vapor qualities and thicker liquid films on the surface, the fins have less influence on the liquid–vapor interface. The heat transfer enhancement with respect to the Reynolds number may result from an interaction between the fins and the turbulence in the liquid film. Low Reynolds number flows may be enhanced more readily than high Reynolds number flows due to the reduction in the size of the turbulent eddies at the wall by the interaction of the flow with the fins. High Reynolds number flows are not enhanced as readily as low Reynolds number flows because there are fewer large eddies to be reduced.

The condensation pressure drop for the micro-fin tube was predicted acceptably well with a modified form of the Pierre (1964) pressure drop correlation for convective evaporation. The hydraulic diameter was used and a new friction factor was developed to account for the fin effect on the flow. The influence of the fin height on the Reynolds number exponent was consist with the Moody chart, suggesting that the surface behaves like a roughness in enhancing the heat transfer.

Acknowledgements

This work was jointly funded by NIST, and the U.S. Department of Energy (project no. DE-AI01-91CE23808) under Project Manager Esher Kweller. Mr. Joaquim Goncalves's NIST sabbatical was funded by CNPq of Brazil (Proj. # 260042/95.1). The authors thank the following NIST personnel for their constructive criticism of the first draft of the manuscript: Mrs. Janet Land, Mrs. Francesca Marchesi, Dr. Vance Payne, and Dr. Jiann Yang. The authors express their appreciation to Mr. Michael Kaul, Mr. Michael Connaghan and Mr. Peter Rothfleisch for their assistance in the construction of the test rig. Furthermore, the authors extend their appreciation to Dr. E. Lagergren and Dr. S. Leigh for their valuable consultations on the uncertainty analysis. Thanks also goes to Wolverine Tube, Inc., for suppling the Turbo-A, micro-fin tube for the test section.

NOMENCLATURE

English Symbols

A_c	cross sectional flow area inside tube (m^2)
A_i	actual inner surface area of tube (m^2)
c_p	specific heat (J/kg·K)
d	number of model parameters
D	tube diameter (m)
D_e	equivalent inner diameter of smooth tube, $\sqrt{4A_c/\pi}$ (m)
D_h	hydraulic diameter of micro-fin tube, (m)
e	height of micro fin (m)
E_h	heat transfer enhancement ratio
f	Fanning friction factor
g	gravitational acceleration, 9.8 m/s^2
G	Mass velocity (kg/m^2·s)
$h_{2\phi}$	local two-phase heat transfer coefficient (W/m^2·K)
h_L	h from linear fit between pure components (W/m^2·K)
i_{fg}	latent heat of vaporization (J/kg)
Ja	refrigerant Jakob Number $i_{fg}/C_{p_{r,l}}\Delta T_s$
k	refrigerant thermal conductivity (W/m·K)
L	tube length (m)
N_f	number of fins
Nu	local Nusselt number based on D_h
$\dot{m}$	mass flow rate (kg/s)
p	wetted perimeter of inner micro-fin tube (m)
P	local fluid pressure (Pa)
Pr	liquid refrigerant Prandtl number $(c_p\mu/k)\|_{r,l}$
q''	local heat flux based on A_i (W/m^2)
Re	all liquid, refrigerant Reynolds number based on $\mathrm{Re} = \mathrm{G}D_h/\mu_{r,l}$
S	perimeter of one fin and channel perpendicular to fin axis (m)
Sv	non-dimensional refrigerant specific volume $((\nu_v - \nu_l)/\nu)\|_r$
T	temperature (K)
U	expanded relative uncertainty
x_q	thermodynamic mass quality
z	axial distance (m)

Greek Symbols

α	helix angle between micro fin and tube axis
β	exponent on correlation
$\Delta h_{2\phi}$	heat transfer degradation (W/m^2·K)
ΔL	incremental length (m)
ΔP	pressure drop (Pa)
ΔT_s	$T_s - T_w$ (K)
Δx_q	quality change over ΔL
μ	dynamic viscosity (kg/m·s)
ν	specific volume, $x_q\nu_v + (1 - x_q)\nu_l$ (m^3/kg)
Φ	two-phase number, $(\Delta x_q\, i_{fg}/\Delta L\, g)$

Subscripts

c	critical condition
f	water
i	inlet, inner
l	liquid
o	exit, outside
p	plain or smooth tube
r	refrigerant
w	heat transfer surface
v	vapor

References

Ackers, W. W. and Rosson, H. F. (1960) Condensation inside a horizontal tube. *Chemical Engineering Process Symposium Series*, **56**(30), 145–149.

Baker, O. (1954) Simultaneous flow of oil and gas, *The Oil and Gas Journal*, **53**, 85–195.

Belsley, D. A., Kuh, E. and Welsch, R. E. (1980) *Regression Diagnostics: Identifying Influential Data and Sources of Collinearity*, New York: Wiley.

Bergles, A. E., Jensen, M. K. and Shome, B. (1995) "Bibliography on Enhancement of Convective Heat and Mass Transfer", HTL-23, Rensselaer Polytechnic Institute, Troy, NY.

Chiang, R. (1993) "Heat Transfer and Pressure Drop During Evaporation and Condensation of Refrigerant-22 in 7.5 mm Diameter Axial and Helical Grooved Tubes", *AIChE Symposium Series No. 295*, **89**, 205–210.

Chamra, L. M. and Webb, R. L. (1995) "Condensation and Evaporation in Micro-Fin Tubes at Equal Saturation Temperatures", *J. of Enhanced Heat Transfer*, **2**, 219–229.

Cooper, M. G. (1984) *Saturation Nucleate Pool Boiling- A Simple Correlation Vol. 86*, Department of Engineering Science, Oxford University, England, 785–793.

Dittus, F. W. and Boelter, L. M. K. (1930) U. CA, *Publ. Eng.*, **2**, 443.

Eckels, S. J., Pate, M. B. and Bemisderfer, C. H. (1992) "Evaporation heat transfer coefficients for R-22 in micro-fin tubes of different configuration", *Enhanced Heat Transfer*, ASME, HTD-Vol. 202, pp. 117–126.

Eckels, S. J., Doerr, T. B. and Pate, M. B. (1994) "In-Tube Heat Transfer and Pressure Drop of R134a and Ester Lubricant Mixtures in a Smooth Tube and Micro-Fin Tube: Part II - Condensation", *ASHRAE Trans.*, **100**, 283–294.

Ghaderi, M., Salehi, M. and Saeedi, M. H. (1995) Review of in-tube condensation heat transfer correlations for smooth and enhanced tubes, Advances in Enhanced Heat/Mass Transfer and Energy Efficiency ASME, HTD-Vol. 320/PID-Vol. 1, pp. 83–94.

Huber, M., Gallagher, J., McLinden, M. and Morrison, G. (1995) NIST Standard Reference Database 23, Version 5.0. Standard Reference Data Program, National Institute of Standards and Technology, Gaithersburg, MD.

Kattan, N., Favret, D. and Thome, J. R. (1995) "R-502 and Two Near-Azeotropic Alternatives: Part I - In Tube Flow-Boiling Tests", *ASHRAE Trans.*, **101**(1), 491–508.

Kaul, M. P., Kedzierski, M. A. and Didion, D. A. (1996) "Horizontal Flow Boiling of Alternative Refrigerants within a Fluid Heated Micro-Fin Tube", *Process, Enhanced and Multiphase Heat Transfer: A Festschrift for A. E. Bergles*, Begell House, Inc., New York, pp. 167–173.

Kedzierski, M. A. and Goncalves, J. M. (1997) "Horizontal Convective condensation of Alternative Refrigerants Within a Micro-Fin Tube", *NISTIR 6095*, U.S. Department of Commerce, Washington, D.C.

Kedzierski, M. A. and Kim, M. S. (1998) "Convective Boiling and Condensation Heat Transfer with a Twisted-Tape Insert for R12, R22, R152a, R134a, R290, R32/R134a, R32/R152a, R290/R134a, R134a/R600a", *Thermal Science and Engineering*, **6**(1), 113–122.

Khanpara, J. C., Bergles, A. E. and Pate, M. B. (1986) "Augmentation of R-113 In-Tube Condensation with Micro-Fin Tubes", *Heat Transfer in Air Conditioning and Refrigeration Equipment*, ASME, HTD-Vol. 65, pp. 21–32.

Koyiama, S., Miyara, A., Takmatsu, H. and Fujii, T. (1990) Condensation heat transfer of binary refrigerant mixtures of R22 and R114 inside a horizontal tube with internal spiral grooves, *International Journal of Refrigeration*, **13**, July, 256–263.

Moody, L. F. (1944) "Friction Factors for Pipe Flow", *ASME Trans.*, **66**, 671–684.

Mori, Y. and Nakayama, W. (1983) "High-Performance Mist Cooled Condensers for Geothermal Binary Cycle Plants", *Heat Transfer in Energy Problems*, Hemisphere, Washington, DC, pp. 211–218.

Muir, E. B. (1989) "Commercial Refrigerants and CFCs", CFCs: Today's Options- Tomorrow's Solutions, *Proceedings of ASHRAE's 1989 CFC Technology Conference*, pp. 81–86.

Pierre, B. (1964) "Flow Resistance with Boiling Refrigerants-Part I", *ASHRAE Journal*, **6**(9), 58–65.

Schlager, L. M., Pate, M. B. and Bergles, A. E. (1989) "Heat Transfer and p876XDrop During Evaporation and Condensation of R22 in Horizontal Micro-Fin Tubes", *Int. J. Refig.*, **12**, 6–14.

Schlager, L. M., Pate, M. B. and Bergles, A. E. (1990) "Evaporation and Condensation Heat Transfer and Pressure Xin Horizontal, 12.7-mm Microfin Tubes with Refrigerant 22", *J. Heat Transfer*, **112**, 1041–1047.

Shah, M. M. (1979) A general correlation for heat transfer during film condensation inside pipes, *International Journal 1926 Heat and Mass Transfer*, **22**, 547–556.

Soliman, H. M. (1982) "On the Annular-to-Wavy Flow Pattern Transition During Condensation Inside Horizontal Tubes", *The Canadian Journal of Chemical Engineering*, **60**, 475–481.

Soliman, H. M. (1983) "Correlation of Mist-to-Annular Transition During Condensation", *The Canadian Journal of Chemical Engineering*, **61**, 178–182.

Soliman, H. M. (1986) "The Mist-Annular Transition During Condensation and its Influence on the Heat Transfer Mechanism", *International Journal of Multi-phase Flow*, **12**(2), 277–288.

Wang, C., Kuo, C. S., Chang, Y. and Lu, D. C. (1996) "Two-Phase Flow Heat Transfer and Friction Characteristics of R-22 and R-407C", *ASHRAE Transactions*, **102**(1), 830–838.

Webb, R. L. (1994) *Principles of Enhanced Heat Transfer*, Wiley Interscience.

Wiegand, J. H. (1945) "Discussion of Paper by McMillen and Larson", *Trans. AIChE*, **41**, 147.